Limit

NASA TECHNICAL TRANSLATION NASA TT F-15803

BUFFETING TESTS WITH A SWEPT WING IN THE TRANSONIC RANGE

B. Monnerie and F. Charpin

Translation of "Essais de buffeting d'une aile en flèche en transonique," Association Aéronautique et Astronautique de France, Colloque d'Aérodynamique Appliquée, 10th, Université de Lille 1, Lille, France, Nov. 7-9, 1973. Paper, 30 pp.

(NASA-TT-F-15803) BUFFETING TESTS WITH A SWEPT WING IN THE TRANSONIC RANGE (Kanner (Leo) Associates) ~~40~~ 39 p HC $5.00 CSCL 01B

N74-28522

Unclas G3/02 43999

NATIONAL AERONAUTICS AND SPACE ADMINISTRATION
WASHINGTON, D.C. 20546 JULY 1974

STANDARD TITLE PAGE

1. Report No. NASA TT F-15,803	2. Government Accession No.	3. Recipient's Catalog No.
4. Title and Subtitle BUFFETING TESTS WITH A SWEPT WING IN THE TRANSONIC RANGE		5. Report Date July 1974 6. Performing Organization Code
7. Author(s) B. Monnerie and F. Charpin, National Office of Aerospace Study and Research, Châtillon-sous-Bagneux, Hauts-de-Seine, France		8. Performing Organization Report No. 10. Work Unit No.
9. Performing Organization Name and Address Leo Kanner Associates Redwood City, California 94063		11. Contract or Grant No. NASw-2481 13. Type of Report and Period Covered Translation
12. Sponsoring Agency Name and Address National Aeronautics and Space Administration, Washington, D.C. 20546		14. Sponsoring Agency Code

15. Supplementary Notes

Translation of "Essais de buffeting d'une aile en flèche en transsonique," Association Aéronautique et Astronautique de France, Colloque d'Aérodynamique Appliquée, 10th, Universite de Lille 1, Lille, France, Nov. 7-9, 1973. Paper, 30 pp.

16. Abstract

A model of the transport-aircraft M6 wing was used to study the characteristics of three-dimensional subsonic and transonic flows in general and the phenomenon of buffeting in particular. In spite of their preliminary tentative nature, the data obtained indicate that the motion of the model has little effect on the aerodynamics and that if this finding is confirmed by future tests with various geometries, it should be possible to study buffeting quantitatively from the nonstationary pressures measured on the wing.

17. Key Words (Selected by Author(s))	18. Distribution Statement
	Unclassified=Unlimited

19. Security Classif. (of this report)	20. Security Classif. (of this page)	21. No. of Pages	22. Price
Unclassified	Unclassified	39	5.00

NASA-HQ

BUFFETING TESTS WITH A SWEPT WING IN THE TRANSONIC RANGE

B. Monnerie and F. Charpin
National Office of Aerospace Study and Research
Chatillon-sous-Bagneux, Hauts-de-Seine, France

1. Introduction /2*

1.1. Review of Goals of M6 Project

The M6 project has been launched by the Aerodynamics Administration of the National Office of Aerospace Study and Research [ONERA] for the purpose of studying three-dimensional flows from low speeds to transonic speeds.

The principal goal is to furnish detailed experimental data, first in order to test present computational methods and to define their validity range, and second, to further comprehension of several complex phenomena, such as tip vortices, airstream separation, boundary layer-shock wave interaction, buffeting, the effect of the Reynolds number, etc., for which available theoretical methods of evaluation are still not completely satisfactory.

1.2. Characteristics of the M6 Wing

It was decided to combine the contour of the M6 wing with that of transonic reference models which have been or about to be tested in various European and American transonic wind tunnels and which have the configuration of a transport aircraft (Fig. 1).

Given the purposes of the experiment, it was important that /3 despite the wall effect which might be expected, the mean chord of the model should be as large as possible in order to obtain

*Numbers in the margin indicate pagination in the foreign text.

realistic Reynolds numbers and so that conditions would be satisfactory for making precise and detailed measurements. For this purpose, the part of the reference models represented was limited to the outer third of the wing. Under these conditions, the principal characteristics adopted for the model (M6 wing) were as follows: aspect ratio 3.8; span 1.2 m; mean chord 0.63 m; sweepback of leading edge 30°; twist 0 (Fig. 2).

The wing was conically generated and the base profile was the ONERA D symmetrical "peaky" profile [1] positioned perpendicular to the plane created by its maximum cross-section. The resultant profile for wing sections created by planes parallel to the wind is given in a table on the next page (p. 3). Finally, it should be noted that the end of the model was equipped with a detachable fairing of revolution.

1.3. Results to be Presented

The initial results of study at low speeds [2] were presented in 1972 at the 9th Colloquium of Applied Aerodynamics of the AAAF. This year the first results of study in the transonic range will be presented. On the basis of a few typical data, the characteristic elements of flow around this wing will be briefly pointed out prior to a detailed examination of the "buffeting" aspect. This is an especially important problem in the transonic range, since the presence of a given buffeting level is frequently the factor limiting the usable flight range for aircraft with Mach numbers close to 1.

2. Study of Flow

2.1. General Remarks

The tests were performed in the S2 Modane Avrieux transonic wind tunnel with variable density and permeability. Taking into

x/l	y/l		x/l	y/l
0.0	0.0		0.3761446	0.0489296
0.0000165	0.0006914		0.4018567	0.0488202
0.0000696	0.0014416		0.4276223	0.0484893
0.0001675	0.0022554		0.4528441	0.0479351
0.0003232	0.0031392		0.4781197	0.0471651
0.0005509	0.0040959		0.5032514	0.0461903
0.0009657	0.0051343		0.5282426	0.0450209
0.0012868	0.0062598		0.5530937	0.0436741
0.0019364	0.0074784		0.5779043	0.0421684
0.0025441	0.0087958		0.6023757	0.0405241
0.0036428	0.0102163		0.6268104	0.0387613
0.0045704	0.0117419		0.6511093	0.0368990
0.0059751	0.0133709		0.6752726	0.0349542
0.0077112	0.0150951		0.6993027	0.0329402
0.0098413	0.0168984		0.7231995	0.0308862
0.0124479	0.0187537		0.7469658	0.0287365
0.0156171	0.0206720		0.7705998	0.0265505
0.0194609	0.0224545		0.7941055	0.0243027
0.0241067	0.0242004		0.8174829	0.0219942
0.0297008	0.0258245		0.8407324	0.0195838
0.0364261	0.0273317		0.8638564	0.0170915
0.0444852	0.0287912		0.8868235	0.0145051
0.0541249	0.0303275		0.9061905	0.0122389
0.0656303	0.0320139		0.9225336	0.0102727
0.0793366	0.0338372		0.9363346	0.0085827
0.0956354	0.0357742		0.9479946	0.0071423
0.1149796	0.0377923		0.9579511	0.0059224
0.1378963	0.0398522		0.9661860	0.0048907
0.1649976	0.0419090		0.9732361	0.0040190
0.1919327	0.0436214		0.9792020	0.0032796
0.2187096	0.0450507		0.9842509	0.0026547
0.2453310	0.0462359		0.9885252	0.0021257
0.2717978	0.0471987		0.9921438	0.0016778
0.2981113	0.0479494		0.9952090	0.0012985
0.3242726	0.0484902		0.9979030	0.0009773
0.3502830	0.0488183		1.0000000	0.0007052

M6 wing: dimensions of profiles of sections parallel to wind.

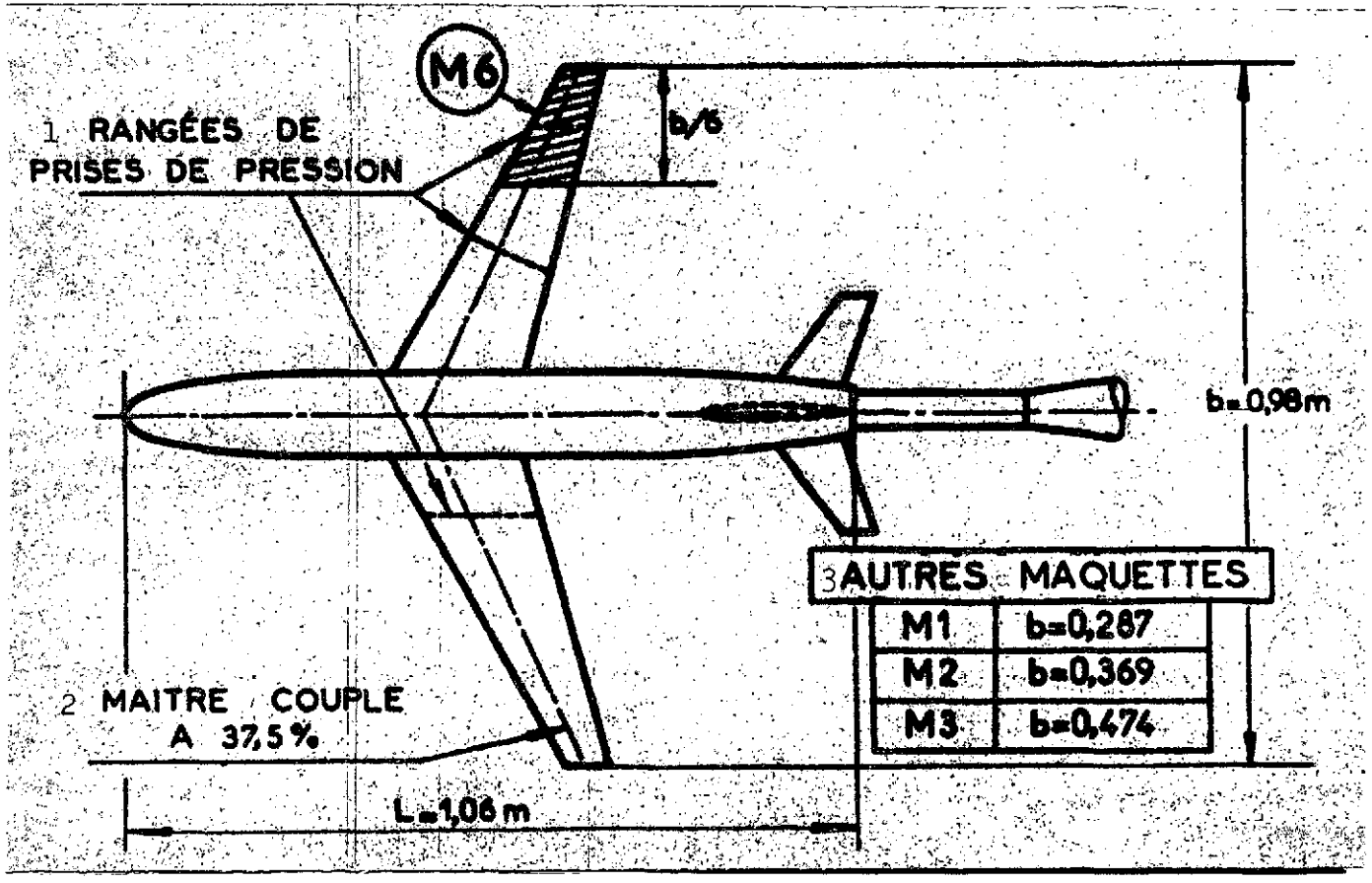

Fig. 1. M5 reference model.

Key: 1. Rows of pressure intakes.
2. Maximum cross-section at 37.5%.
3. Other models.

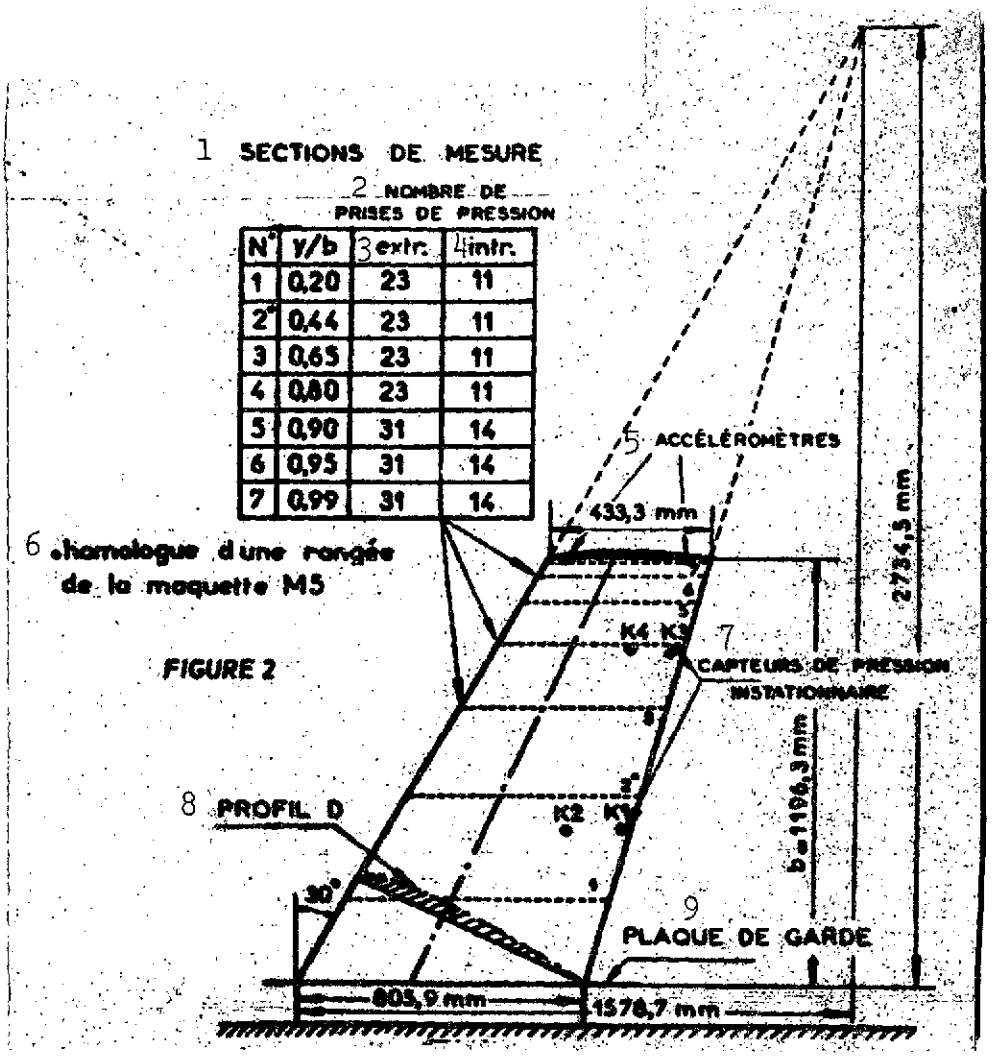
1 SECTIONS DE MESURE
2 NOMBRE DE PRISES DE PRESSION
N° | y/b | 3 extr. | 4 intr.
1 | 0,20 | 23 | 11
2 | 0,44 | 23 | 11
3 | 0,65 | 23 | 11
4 | 0,80 | 23 | 11
5 | 0,90 | 31 | 14
6 | 0,95 | 31 | 14
7 | 0,99 | 31 | 14
6 .homologue d une rangée de la maquette M5
5 ACCÉLÉROMÈTRES
433,3 mm
2734,5 mm
K4 K3
7
CAPTEURS DE PRESSION INSTATIONNAIRE
b=1196,3 mm
8 PROFIL D
K2 K1
30°
9
PLAQUE DE GARDE
805,9 mm
1578,7 mm

FIGURE 2

Fig. 2. M6 wing.

Key: 1. Measurement sections.
2. Number of pressure intakes.
3. Outer.
4. Inner.
5. Accelerometers.
6. Homologous to a row on the M5 model.
7. Nonstationary pressure sensors.
8. D profile.
9. Guard plate.

account the considerable blockage produced by the model, the permeability was adjusted for the test to a maximum rate of 6% (average permeability, since only the horizontal walls were perforated).

Unless otherwise stated, the data given were obtained with natural transition.

2.2. Pressure Measurements

The wing contained 270 pressure intakes distributed among seven sections parallel to the wind (Fig. 2). The measurements were performed by means of pressure distributors.

2.2.1. Data Obtained at Zero Angle of Attack

Fig. 3 shows variations in pressure distribution at zero angle of attack as a function of Mach number for sections located at a distance from the wing root equal to 44% and 90% of the span.

The curves, which are based on raw data which have not been corrected for the wall effect, give the ratio of the measured pressure to the generating pressure of the wind tunnel as a function of a reduced abscissa XR = (X - leading edge X)/local chord. This expression will be used systematically in the following discussion. /4

Let us first take a look at the test data for the section close to the semi-span. At a Mach number of 0.5, the pressure distribution is analogous to that which has been observed with incompressible [waves?] for "peaky" profiles at zero angle of attack with a small overspeed peak slightly behind the leading edge, followed by a pressure plateau and slow recompression up to the trailing edge. As the Mach number is increased, the pressure jump corresponding to the overspeed peak increases fairly sharply,

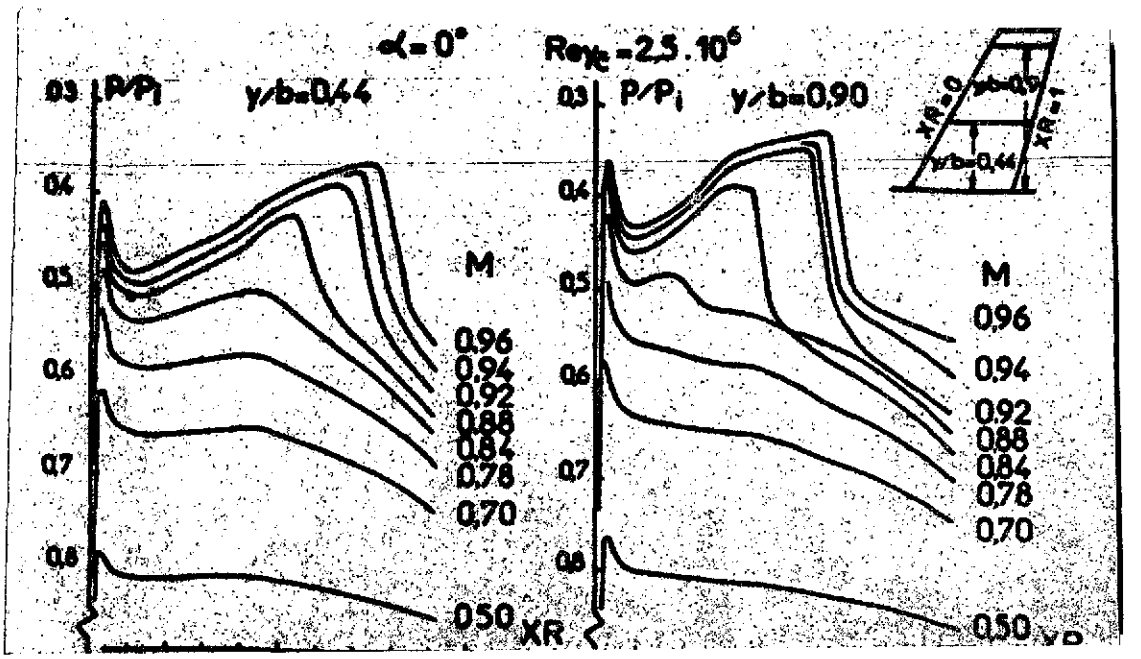

Fig. 3. Pressure distribution. $\alpha = 0°$. $R_{\bar{c}} = 2.5 \cdot 10^6$.

and then stabilizes. The leading edge reaches the speed of sound at an upstream Mach number of approximately 0.78. At around Mach 0.86, an impact is produced toward the middle of the airfoil and quickly recoils (that is, shifts toward the rear of the airfoil), to be located at 80% of the chord toward Mach 0.96.

The pressure distribution of the tip section varies qualitatively in the same manner as that for the mean section, but in detail their variations are relatively different.

The pressure minimum at the same Mach number is more marked for the tip section than for the mean section, and as a result the critical Mach number is lower (0.75). Since, on the other hand, the levels of trailing edge pressure are identical, at least

at low Mach numbers, there is no longer a plateau, but a continuous recompression of the leading edge toward the trailing edge.

The second impact originates closer to the leading edge toward Mach 0.82; thus, despite fast recoil, this impact is at only 65% of the chord at Mach 0.96.

To obtain a precise idea of the three-dimensional effects, a curve was plotted (shown in Fig. 4) giving the pressure distribution over the wingspan at a relative depth of 0.1, which corresponded to points located immediately upstream from the overspeed peak.

At low Mach numbers, as well as extremely low speeds [2], the curve is roughly isobaric. The flow is pseudo-two-dimensional and the data may be compared to those obtained with planar flow for large parts of the wing.

This is no longer true in the transonic range. As soon as a critical Mach number is approached, the three-dimensional effects become considerable even though the wing is symmetrical and its angle of attack is zero.

Fig. 5 corroborates this finding, giving an approximate curve for the position of the rear impact at three Mach numbers: for Mach 0.88 the position of the impact changes from 65%, close to the wing root, to 20%, close to the tip.

2.2.2. Data Obtained at Angles of Attack of 3° and 6°

Let us now examine the data obtained by increasing the angle of attack.

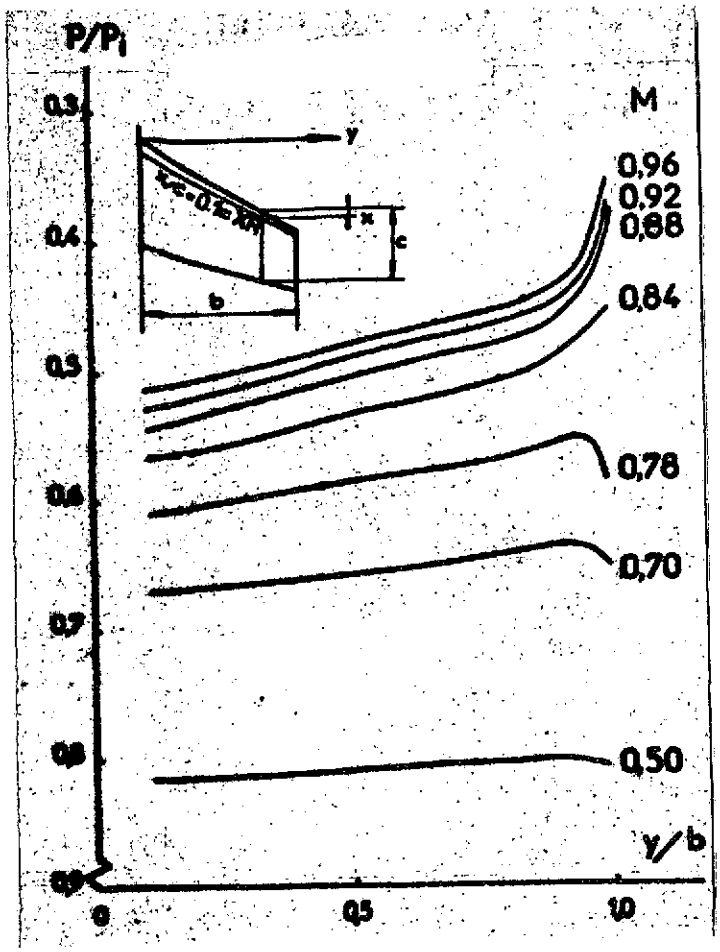

Fig. 4. Pressure distribution at a relative depth of 0.1. $R_c = 2.5 \cdot 10^6$. $\alpha = 0°$.

Fig. 6 shows pressure distribution on the top skin of sections 2 and 4 (y/b = 0.44 and 0.8) for an angle of attack of 3°. /5

In the mean section, an intense impact related to the "peaky" nature of the wing profile occurs close to the leading edge at both Mach numbers. This impact recoils as the Mach number increases and its intensity simultaneously decreases.

At approximately Mach 0.8, a second impact originates toward the maximum cross-section. It also recoils as the Mach number increases, but its intensity increases, producing airstream separation at the rear of the airfoil at high Mach numbers, a phenomenon whose presence is indicated by the low pressure level attained at the trailing edge at Mach 0.96.

The development is similar in the section close to the tip, but the leading edge impact moves farther toward the rear. The impact quickly recoils, becoming attenuated, and disappears completely at Mach 0.96.

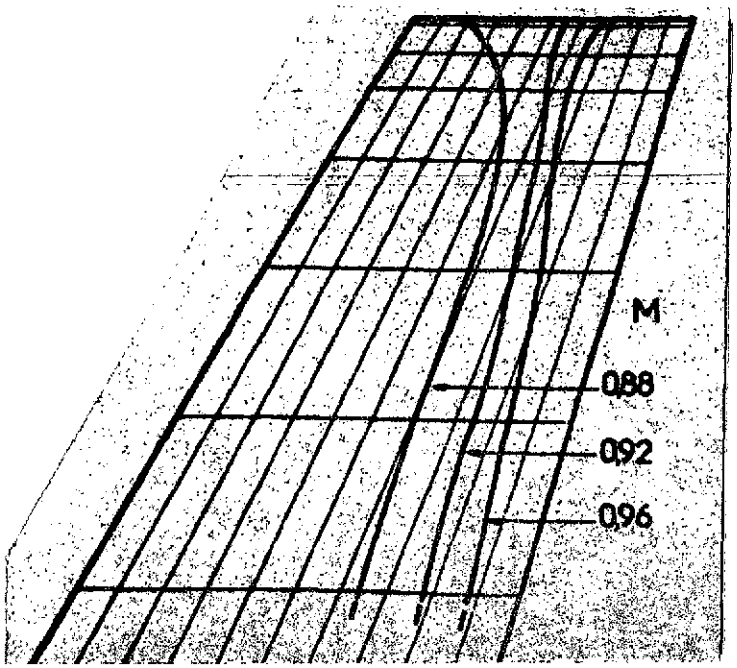

Fig. 5. Position of rear impact.
$\alpha = 0°$. $R_{\bar{c}} = 2.5 \cdot 10^6$.

At large angles of attack (6°), as shown in Fig. 7, it may be noted that the behavior of the mean section is identical to that of the section close to the tip at 3°: the leading edge impact recoils quickly and becomes attenuated, almost disappearing at Mach 0.96 and resulting in distribution by a single impact.

In section 4 (y/b = 0.8), there is no longer any distribution by a single high-intensity impact. As the Mach number increases, this impact recoils and produces a separation of the airstream from the rear of the airfoil beginning at Mach 0.84. This finding may already be confirmed by examining the pressure levels reached at the leading edge by comparison with those obtained on the mean section, but this point will be analyzed in greater detail in Part 3.

The preceding statements may be clarified by a look at Figs. 8 and 9, where the positions of the impacts obtained are plotted as a function of the pressure distribution in the seven sections at 3° and 6° from Mach 0.84 to 0.92.

At 3°, the forward impact and the rear impact observed in the vicinity of the root converge toward the tip of the wing; they

come to coincide at 90% of the span, both at Mach 0.84 and at Mach 0.92.

At 6°, the forward impact has recoiled, pivoting approximately about the apex, while the rear impact has shifted very little. As a result these impacts come to coincide closer to the root at 70% of the wingspan, and this explains why pressure distributions with no impact are obtained in section y/b = 0.8 at 6°.

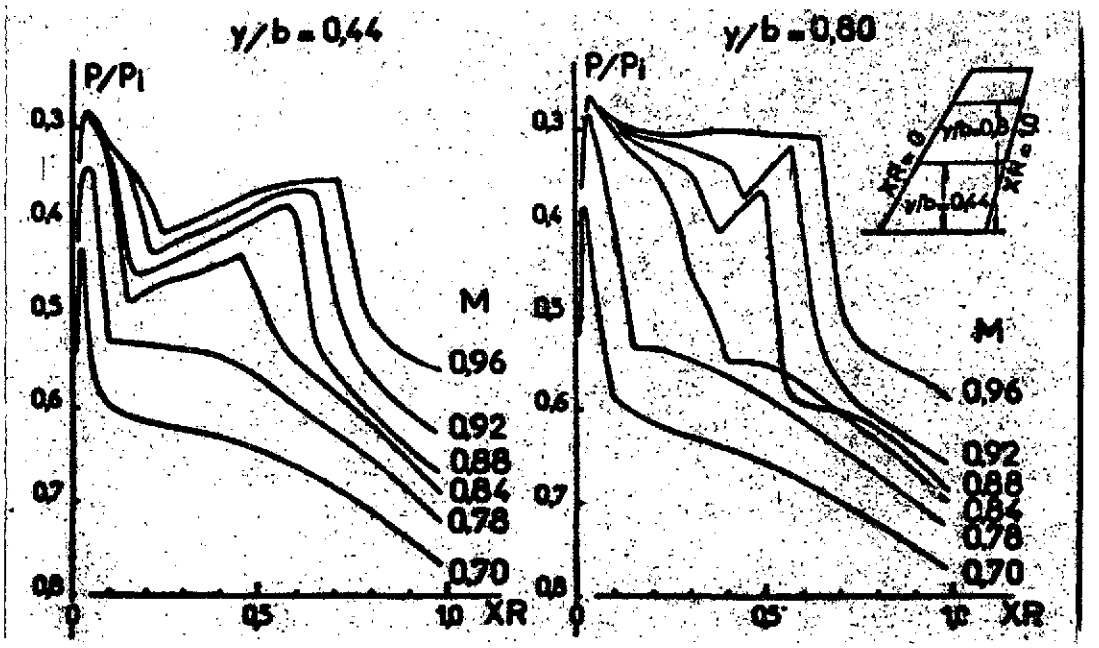

Fig. 6. Pressure distribution on outer skin.
$\alpha = 3°$. $R_{\bar{c}} = 2.5 \cdot 10^6$.

2.3. Stained Parietal Visualization

Confirmation of the preceding curves was furnished by stained parietal visualization (Plate 1).

This was accomplished by injecting an extremely fluid mixture composed of equal parts kerosene and carbon diphenyltetrachloride, and stained with colored pigments, into openings machined in the

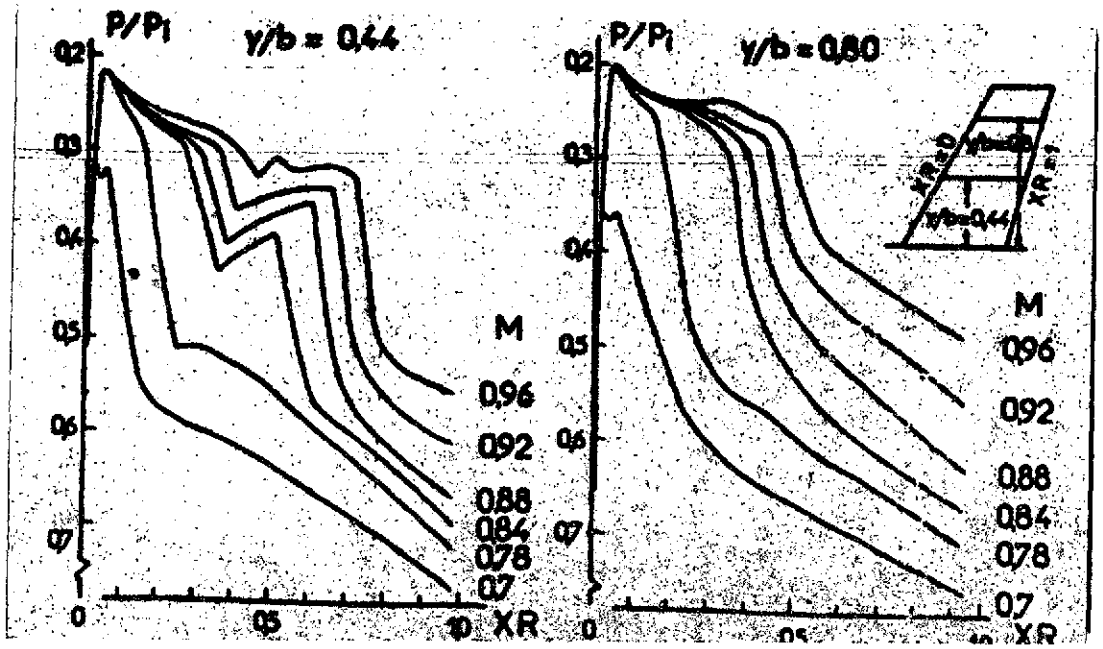

Fig. 7. Pressure distribution on outer skin.
$\alpha = 6°$. $R_{\bar{c}} = 2.5 \cdot 10^6$.

wall to perform pressure measurements.

Photographs and a film were made during the tests. Due to /6
the fact that pure kerosene was being fed into the injection openings, it was possible to clean the model without having to interrupt the air current. Thus it was possible to obtain a large number of photographs for different test conditions (variations as a function of angle of attack, Mach number and Reynolds number) in a relatively short period of time.

This technique permitted a precise determination of the pattern of parietal current lines; for example, a change in direction may be observed as the impacts pass over the wing. The technique is particularly spectacular for visualization of air-

stream separation due to the accumulation and recirculation zones produced by this phenomenon.

In the case of Plate 1, where the Reynolds number is relatively low, the flow is laminar up to the first impact (this finding will be demonstrated later), and the boundary layer-shock wave interaction results in an impact base separation. The stained fluid furnishes satisfactory visualization of this phenomenon, which provides information on the position of the impact. It may be assumed that the trace of the impact on the wing is located at the upstream limit of the stained area, an assumption which is confirmed by cross-checking performed on the measurement sections to obtain the pressure distribution.

2.4. Influence of Reynolds Number

One of the largest problems in transonic simulation is attempting to set the Reynolds number which should be attained so that it will be possible to predict in-flight performance with precision. Considerable differences may be found between wind tunnel test data and flight data when the Reynolds number used for the wind tunnel tests is too low. There may be a high degree of risk in extrapolating these data without precautionary measures, since there may be changes in flow speed between the Reynolds numbers attained and those for which knowledge of flight characteristics is desired.

Furthermore, use of the transition triggering techniques designed to preclude changes in speed is fairly complex, since at the very least, a boundary layer with the same relative thickness as that obtained in flight must be reconstructed upstream from the initial impacts, necessitating adjustment of the triggering devices for each test case (angle of attack, Mach number, Reynolds number).

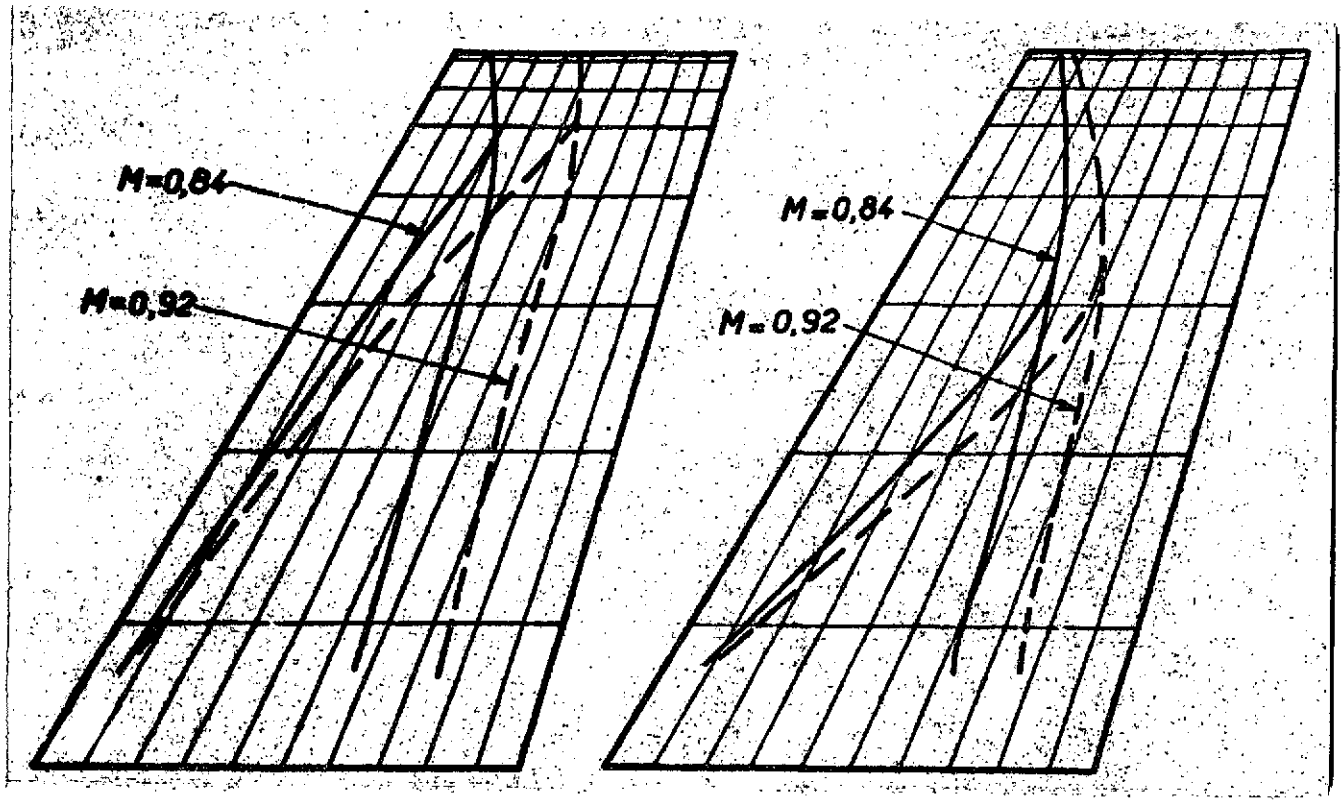

Fig. 8. Fig. 9.

Figs. 8 and 9. Impact curves.
$\alpha = 3°$. $R_c = 2.5 \cdot 10^6$ $\alpha = 6°$.

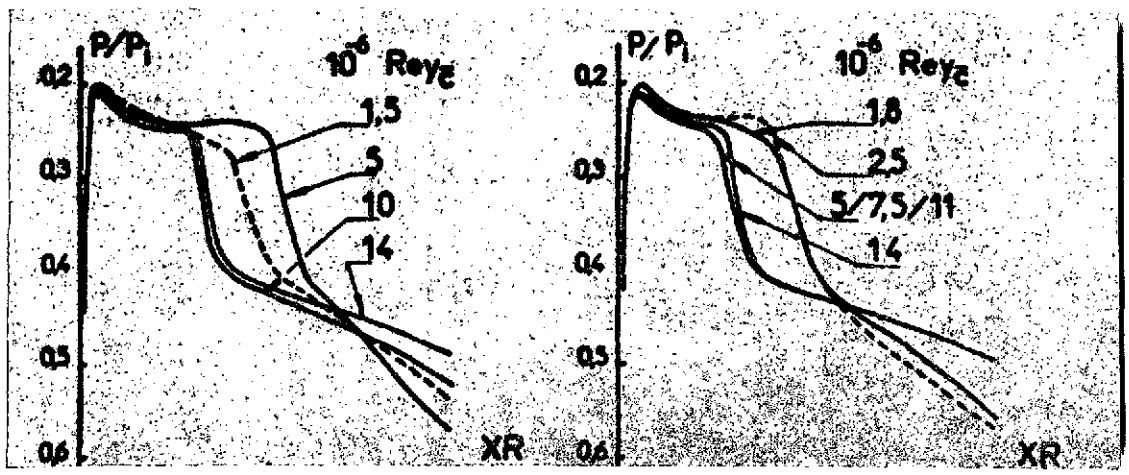

a) Natural transition. b) Triggered transition.

Fig. 10. Influence of Reynolds number. M = 0.92. $\alpha = 6°$. $\bar{y}/b = 0.8$.

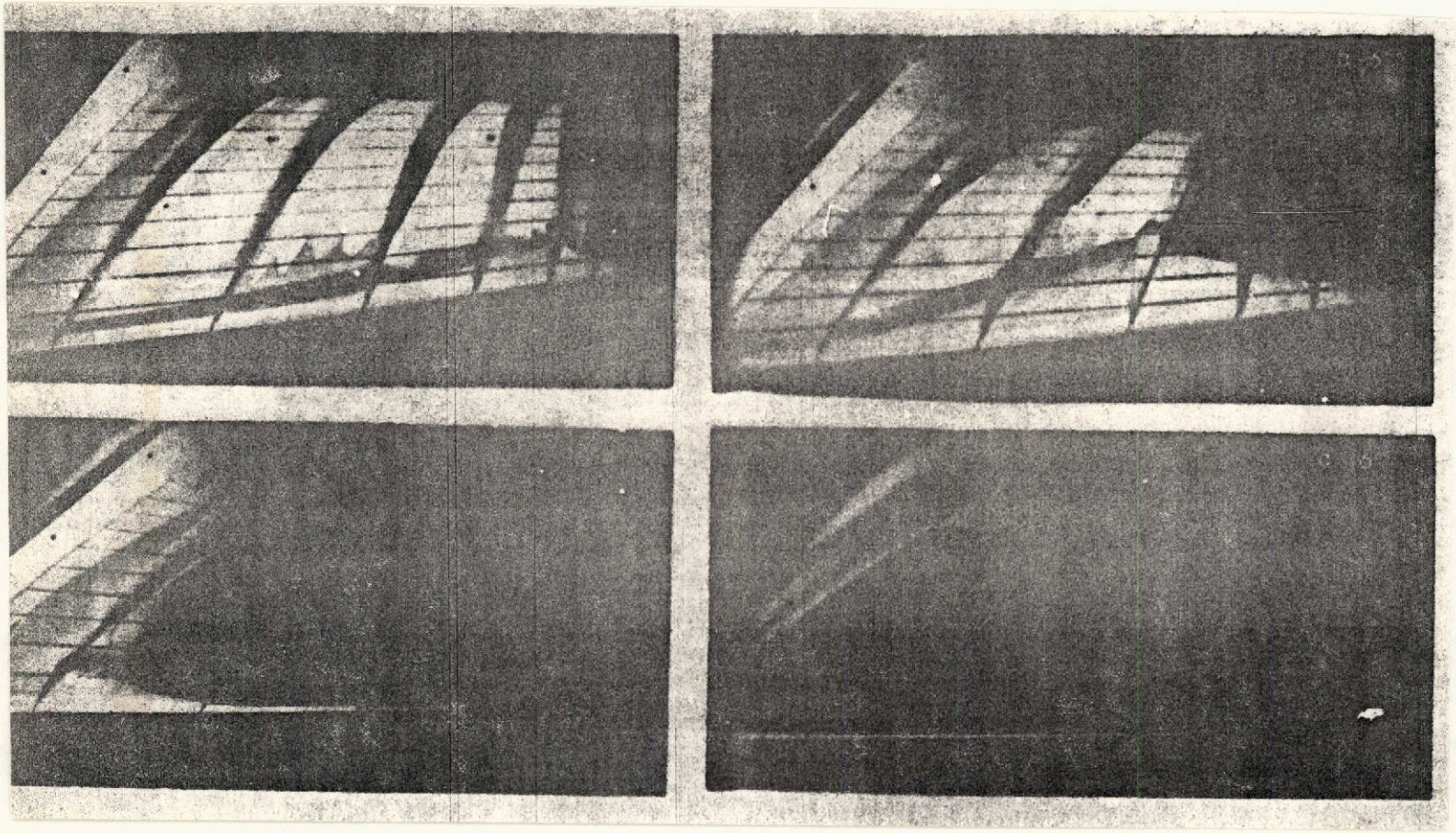

Plate 1. Parietal visualizations.
$M = 0.84$. $R_{\bar{c}} = 2.5 \cdot 10^6$.

The M6 wing is an excellent tool for clarification of this difficult problem, since it offers the possibility of varying the Reynolds number in relation to the mean chord, from 1.5 million, a value close to those commonly attained in wind tunnels for three-dimensional models, upto relatively high values (10 to 15 million).

No detailed and systematic analysis of the Reynolds effect on the M6 wing has yet been performed, but it is possible to point out a few tendencies drawn from our initial observations:

-- The effect of an increase in the Reynolds number is slight and is generally favorable in any case in which the transition position is set relatively close to the leading edge by sufficient recompression to produce laminar separation.

-- When this condition is not met, as is frequently the case when the Mach number approaches 1, the effect of an increase in Reynolds number may be very marked and unfavorable, as the result of a considerable upstream shift in the transition position. In this case the effect of the Reynolds number becomes favorable once again only beyond high Reynolds number values, when the /7 transition is no longer able to shift forward since it is occurring on the leading edge.

An example illustrating the latter case is given in the righthand diagram in Fig. 10. At Mach 0.92 and an angle of attack of 6°, as the Reynolds number increases the impact detected by means of measurements performed in section (y/b = 0.8) begins to recoil. When the Reynolds number reaches 5 million, it suddenly moves forward and begins to shift to the rear once again only after 10 million has been reached (Fig. 11). This rapid forward shift of the impact is explained by a shift in the transition position; this may be seen in Plates 2 and 3, which show, for

Reynolds numbers of 2.5 and 11 million; in (a), stained parietal visualizations, and in (b) and (c), visualizations of the transition position by means of acenaphthene sublimation [general view in (c) and close-up view of leading edge area in (b)].

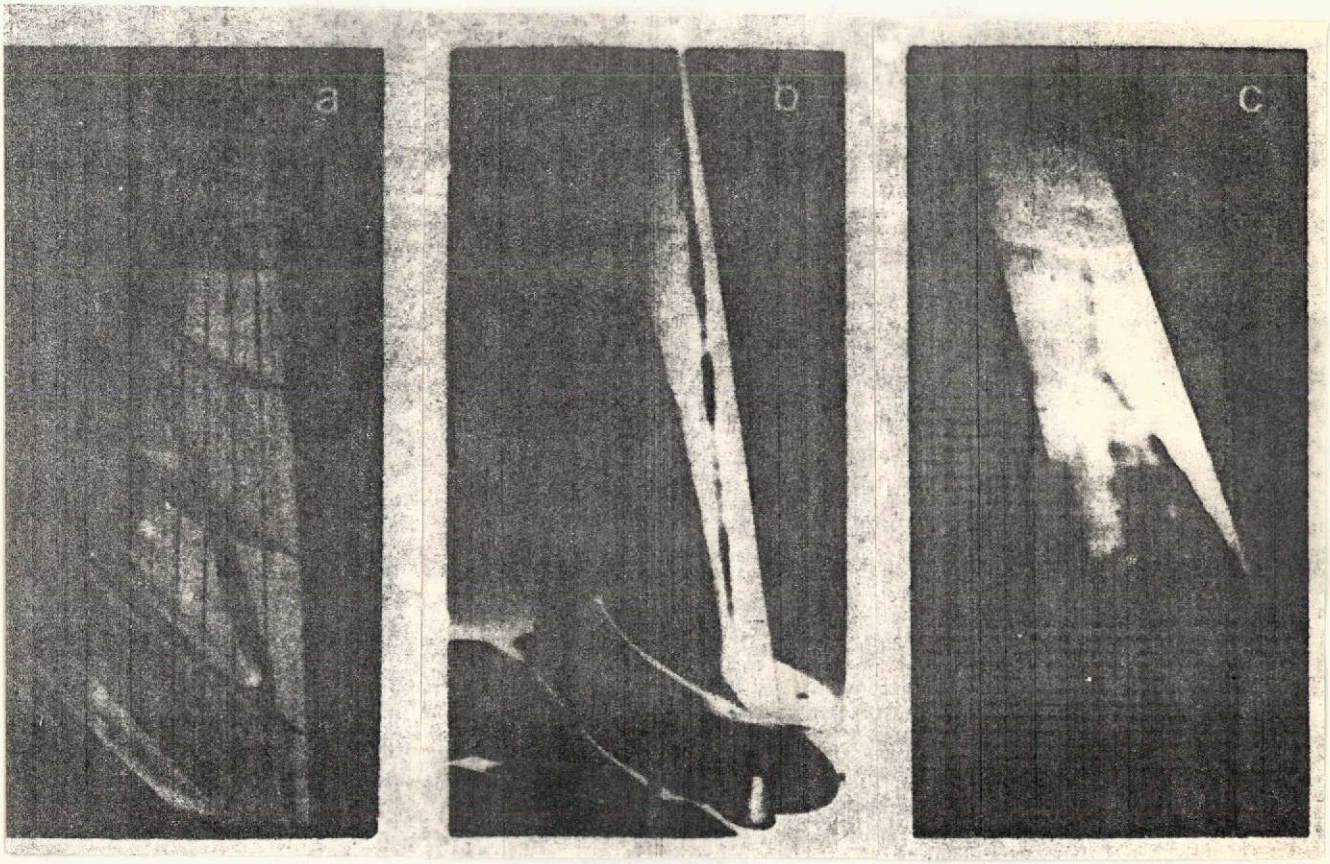

Plate 2. Parietal visualizations.
$M = 0.92$. $R_{\bar{c}} = 2.5 \cdot 10^6$. $\alpha = 6°$.

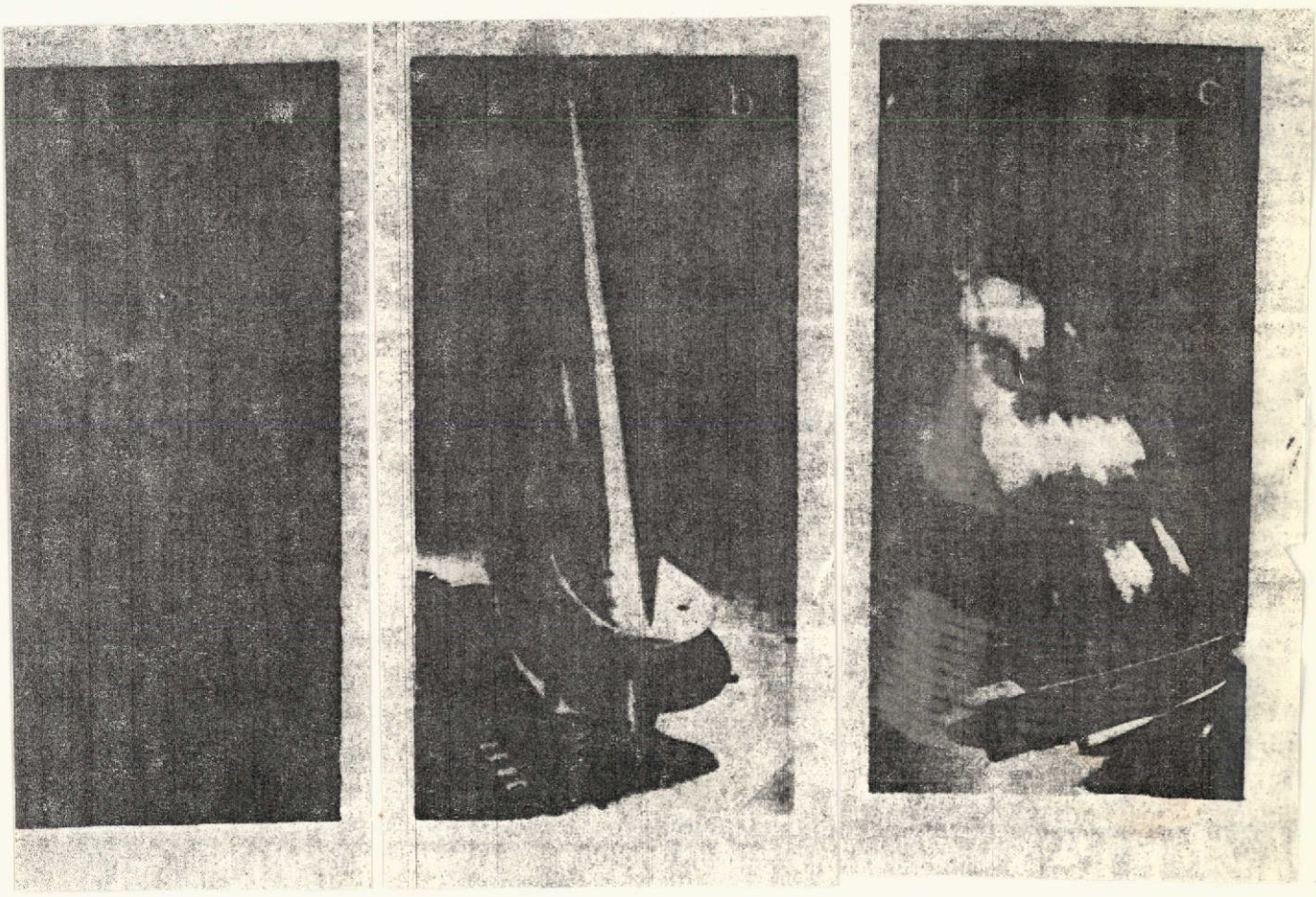

Plate 3. Parietal visualizations. $M = 0.92$. $R_{\bar{c}} = 11 \cdot 10^6$. $\alpha = 6°$.

At a low Mach number (Plate 2), the flow remains laminar up to the impact. The laminar separation due to the impact produces the transition, and precise comparison shows that there is satisfactory agreement between the upstream limit and the separated impact base zone detected in visualizations (a) and the transition position visible in (c).

At a high Mach number (Plate 3), the transition occurs at the level of the maximum speed immediately behind the leading edge, except in the immediate vicinity of the wing root. Under these conditions, the boundary layer arriving at the level of the impacts emanating from the apex of the wing is turbulent, and there is no impact base separation as previously. Only a slight break in the flow lines as they pass through the impact may be noted in Photograph (a).

The effect of the shift in the transition is particularly notable here, since the flow has a tendency to separate in the vicinity of the trailing edge, and the increase in thickness of the boundary layer attendant on the upstream shift in the transition position increases the extent of the separation.

Finally, it may be noted that we have performed a few tests with artificial triggering of the transition (a strip of spherical balls with a diameter of 0.1 mm, placed on the wing between lines XR = 0.04 and 0.05). Acenaphthene visualizations showed that the transition occurs at the level of the roughness for a Reynolds number of 5 million; this is not the case at lower Reynolds numbers. (At 2.5 million, for example, the transition occurs at approximately 15% of the relative depth.) It therefore follows that the change in flow speed noted with natural transition between 5 and 10 million occurs at lower Reynolds numbers, between 2.5 and 5 million, due to the roughness. (Figs. 10 b and 11).

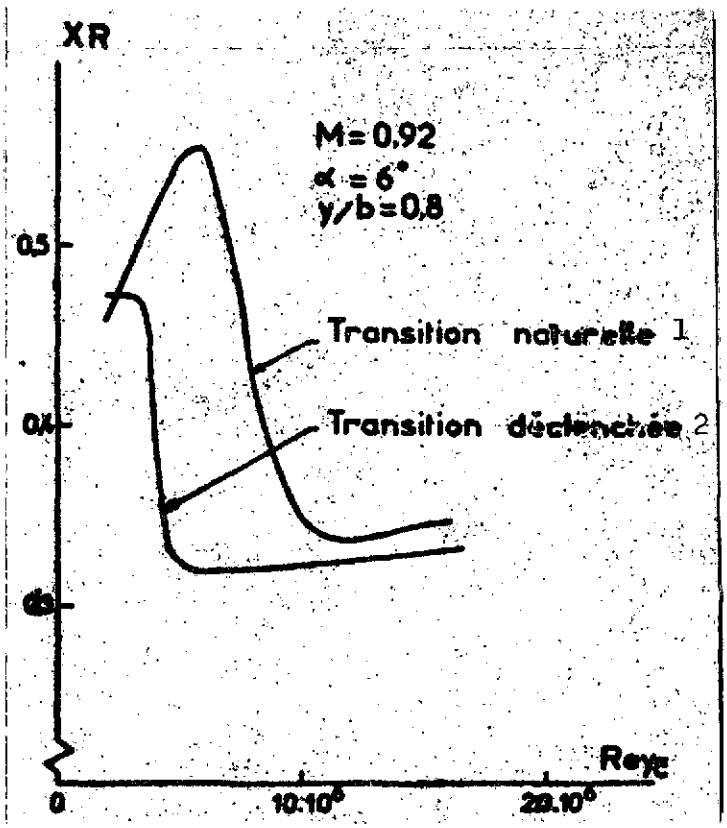

Fig. 11. Influence of Reynolds number on position of impact.

Key: 1. Natural transition.
2. Triggered transition.

3. Study of Buffeting

3.1. General Remarks

One of the major problems presented by aircraft flight in the transonic range is buffeting. This phenomenon consists in vibration of the aircraft which may be detected by the pilot and passengers in certain flight configurations. Buffeting is not specific to the transonic range, since it may occur at low speeds prior to stall, but it is more often mentioned with reference to the transonic range, since in this range it may occur well before stall and its intensity may be considerable. Flight under these conditions is unacceptable both for the passengers and for the aircraft structure, and the flight range limit frequently corresponds to the limit at which a given level of buffeting occurs. This fact indicates the importance of wind tunnel methods for detecting and quantizing buffeting. /8

It may fairly quickly be seen that buffeting is directly linked to the occurrence around the aircraft of separated airflow zones with a given degree of extension. The phenomenon thus involves

both aerodynamics and structure.

It is readily apparent that the aerodynamics has a direct influence on the movement of the structure; the problem which must be solved is to what degree the structure influences the aerodynamics. If this influence is considerable, wind tunnel buffeting tests should be performed in the same way as flutter tests, using models with dynamics similar to the aircraft. This would be a serious, if not insurmountable, technical problem, since these models should be able to operate under heavy loads.

The first goal which may be set is to determine when buffeting first occurs in wind tunnel tests. In this case, since a threshold must be determined, the movement of the model will at any rate be imperceptible, and one may expect to obtain significant data, even with a rigid model, provided that the aerodynamic phenomena are closely similar to those occurring in flight.

The second objective will be to attempt to determine the influence of movement of the model on the aerodynamics.

The methods for detecting buffeting are based either on direct measurement of the responses of the structures or on any method making it possible to estimate the presence and extent of separated zones on the model. As a result, a large number of methods are available; these may be divided into two categories.

The first category includes:

-- use of accelerometers,

-- methods permitting measurement of fluctuations in the overall stresses exerted on the model (lift, roll, pitching moment),

-- [illegible]

and in the second category:

-- pressure divergence on the trailing edge,

-- measurement of pressure fluctuations,

-- visualization techniques,

-- analysis of breaks in the overall stress curves (CL, CD, Cm and C_1).

3.2. Description of Test Performed on M6 Wing /9

From the first group of methods listed above, we chose the use of accelerometers placed at the wing tip to detect movements perpendicular to the plane of symmetry of the wings (see Fig. 2) and measurement of fluctuations in the wing bending moment. Methods used from the second group were determination of trailing edge pressure divergence in the seven measurement sections of the model and measurement of pressure fluctuations at four points located in the rear part of the wing at 75% and 98.5% of the relative depth, using Kulite LQL 08025 sensors with flush membranes (see Fig. 2).

The other methods may furnish significant data, but they appeared to us to be less direct or less precise than the methods used. Vizualizations, for example, would have been quite helpful in interpreting the data, but it is not always easy to give a precise determination of the exact limit of some separated zones.

Instead, a microphone located on the wall of the wind tunnel upstream from the experimental airflow furnished information on the level of fluctuations present in the incident flow.

The measurement channels making it possible to process the various nonstationary signals included the following components (see Fig. 12):

-- an initial Al amplifier to increase the level of the signal and to adapt the impedance prior to input into the filter,

Reproduced from best available copy.

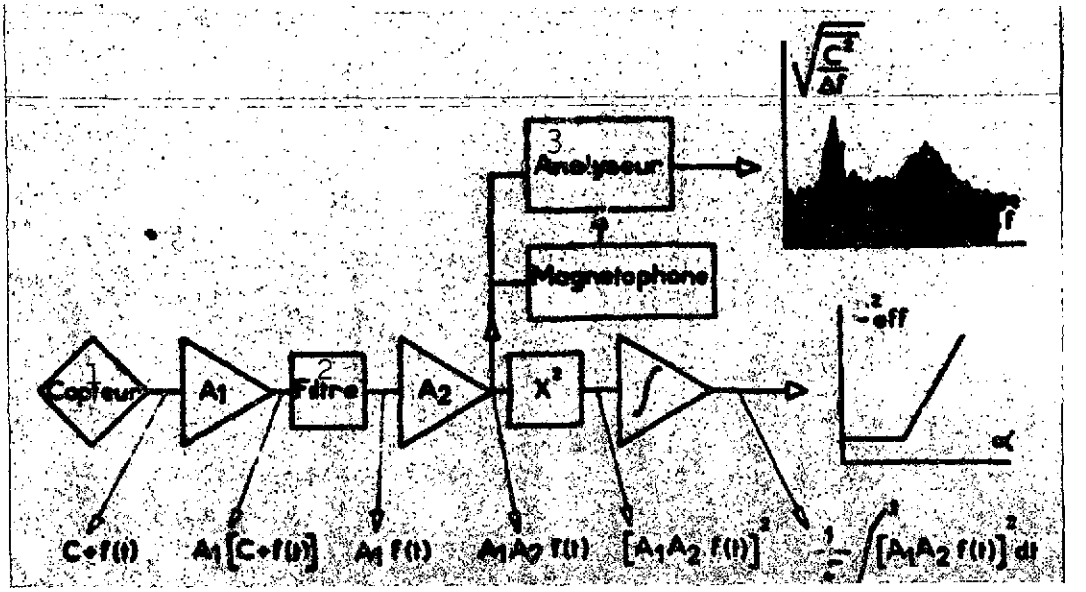

Fig. 12. Nonstationary measurements.

Key: 1. Sensor. 2. Filter. 3. Analyzer.

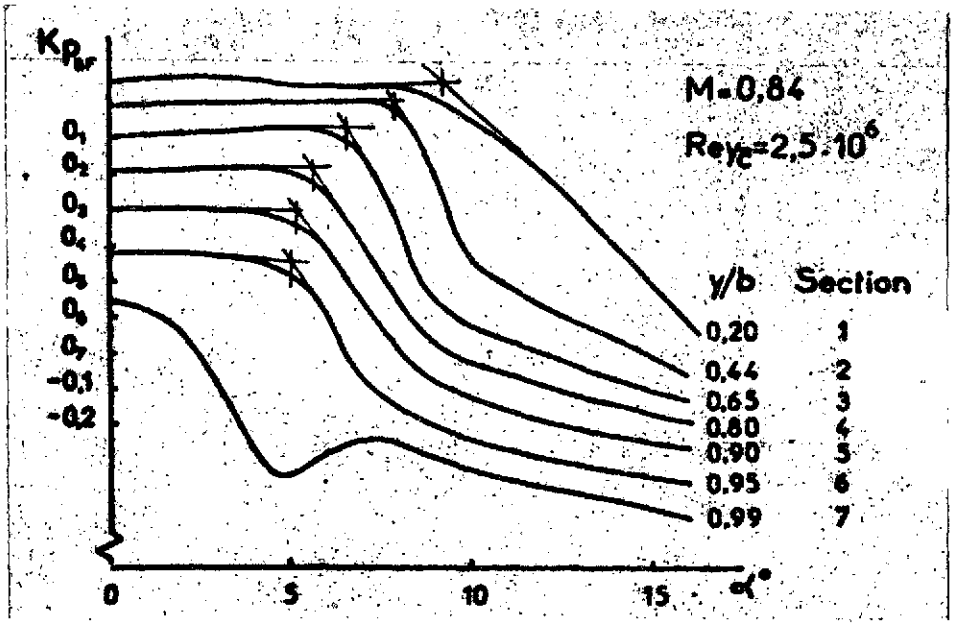

Fig. 13. Variations in trailing edge pressure as a function of angle of attack.

PRECEDING PAGE BLANK NOT FILMED

-- an RC high-pass filter eliminating the continuous component (cut-off frequency 0.3 Hz),

-- a second amplifier,

-- a multiplier giving the square of the dynamic signal,

-- an analog integrator with digital output (integration time adjusted to 10 sec).

It was thus possible to obtain the square of the effective value of various signals in real time.

In parallel on the preceding string, a spectral analyzer in real time traced the amplitude spectrum of one of the channels and the entire series of analog signals was recorded on a magnetophone for complete processing in deferred time.

3.3. Presentation of Data

3.3.1. Pressure Divergence at Trailing Edge

An example of variations in pressure in the vicinity of the trailing edge (XR = 0.985) as a function of the angle of attack is given in Fig. 13 for a Mach number of 0.84. It may be noted that, except in the special case of the tip section, the pressure remains constant as the angle of attack increases from 0, and then after a short transitional period begins to increase fairly rapidly; that is, it "diverges."

Correlation with other methods of investigation, such as visualization techniques or wake sensing, shows that this rapid increase is produced by the occurrence of a separation at the trailing edge. The separation appears at the tip towards 5° and extends over the wingspan as the angle of attack increases. It reaches section 1 toward 9°. Fig. 14 shows the angle of attack for diverging pressure at the trailing edge as a function of the position along the wingspan for several Mach numbers. It may be /10

noted that the time it takes the separation to occur at the tip is prolonged as the Mach number increases.

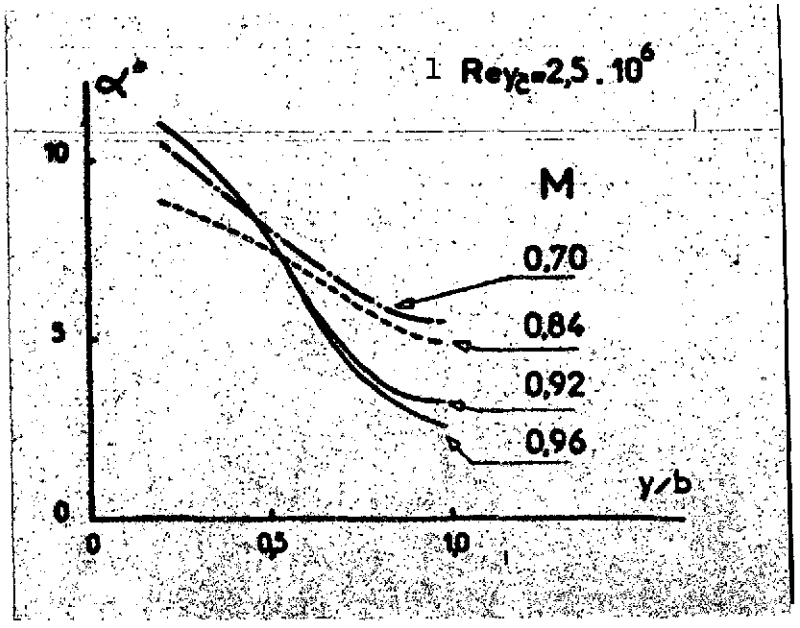

Fig. 14. Angle of attack for diverging $K\bar{p}_{te}$ as a function of wingspan.

Key: 1. $R_c = 2.5 \cdot 10^6$.

3.3.2. Use of Rate of Pressure Fluctuation

The lower diagram in Fig. 15 shows the ratio of variations in the square of the effective pressure value to the square of the dynamic pressure, as a function of the angle of attack, for sensors and K1 and K3 placed in the vicinity of the trailing edge, at 36% and 78% of the wingspan, respectively. (The effective value is the root mean square pressure variation over time, the pressure variation being denoted by Δp, that is:

$$\sqrt{\overline{\Delta p^2}} = \sqrt{\frac{1}{\tau}\int_0^{\tau} \Delta p^2 \, dt} \quad \text{with} \quad \Delta p = p - \frac{1}{\tau}\int_0^{\tau} p \, dt$$

The variation is identical to that observed in the preceding section for the trailing edge pressure. The rate of fluctuation is slight and constant at a small angle of attack, and it increases

suddenly beginning at a given angle of attack. Moreover, the angle at which this increase occurs exactly corresponds to the angle of attack for pressure divergence at the trailing edge. This may be confirmed by examining the curve in Fig. 14 for a Mach number of 0.84, reproduced at the top of Fig. 15.

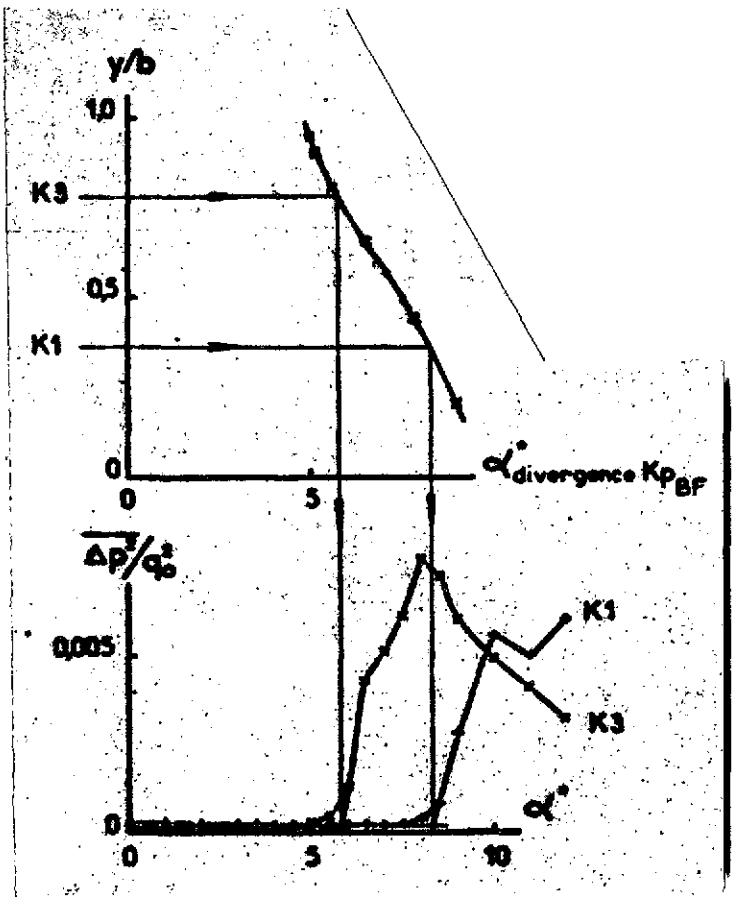

Fig. 15. Relationship between stationary and nonstationary pressure. M = 0.84. $R_c = 2.5 \cdot 10^6$.

Before proceeding to an analysis of the other dynamic signals, it should be noted that the rate of fluctuation received by sensor K3, placed at 78% of the wingspan, reached a maximum and then decreased fairly sharply, seeming to indicate some degree of stabilization in the airstream separation. This should be compared to the parietal visualizations given in Plate 1, which show a

clearly organized separation at the wing tip at 10°and 16°.

3.3.3. Use of Responses of Structures

Variations in the square of the effective value of the bending moment in relation to the wing root and the acceleration at the tip, as a function of the angle of attack, are given for Mach 0.84 by Fig. 16. As previously, there is a sudden increase beginning at a given angle of attack.

Lines drawn in from previous graphs make it possible to compare the divergence angles of attack for the various effective values. The divergence in $\Delta F \cdot V^2$ appears slightly later (0.5°) than divergence in the effective pressure value at 78% of the span, and much later (1.5°) than the divergence shown on the accelerometer.

3.3.4. Comparison of Methods

The angles of attack obtained for divergence with the various methods used are given as a function Mach number in Fig. 17.

The curves representing the trailing edge pressure at y/b = 0.95 and the nonstationary pressures at y/b = 0.78 and 0.36 obviously follow stages as a function of the angle of attack, since a separation originates at the tip and extends toward the root as the angle of attack increases. The angle at which separation first occurs thus increases as the wing root is approached. The wing bending bridge signals the onset of buffeting at virtually the same time as the nonstationary sensor at 78%. Thus the separation must cover a sizable fraction of the wing (20-25%) in order to be detected at the root.

On the other hand, the Al accelerometer is able to detect buffeting at an earlier stage than the trailing edge intake at y/b =

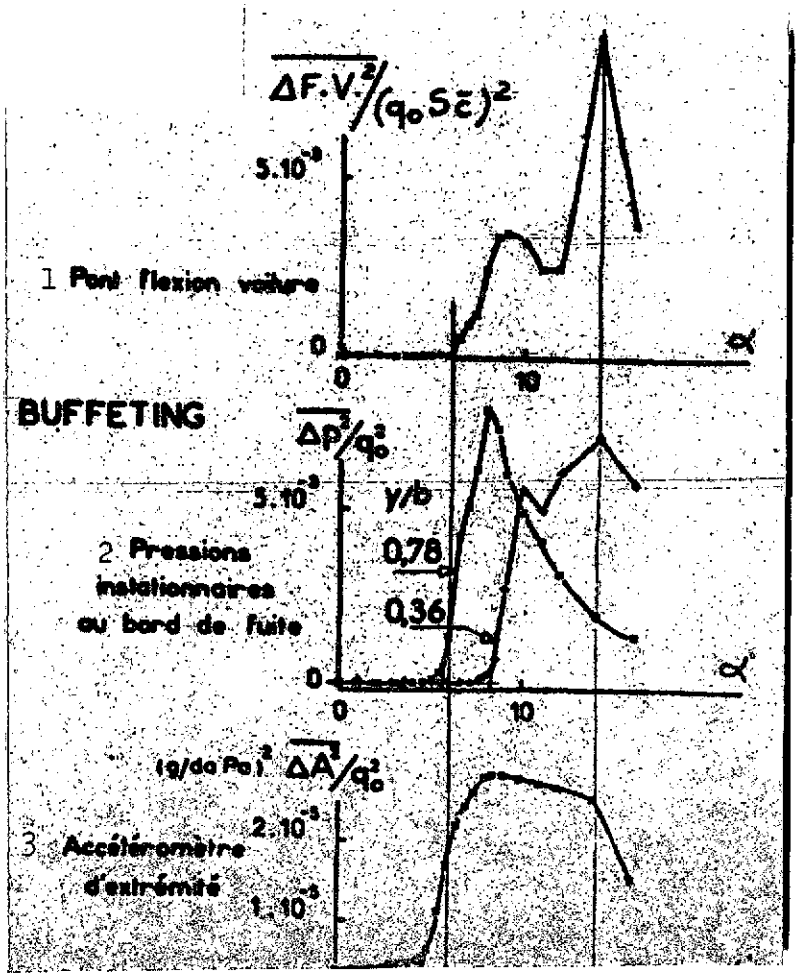

Fig. 16. Study of onset of buffeting. $M = 0.84$. $R_{\bar{c}} = 2.5 \cdot 10^6$.

Key: 1. Wing bending bridge.
2. Nonstationary pressures at trailing edge.
3. Accelerometer at tip.

0.95. Thus some separation must be localized in the the immediate vicinity of the tip, resulting in very early activation of the accelerometers placed in this location.

Finally, the decrease in the buffeting limit as the Mach number increases should be noted. This is related to the increase in intensity of impacts as the Mach number increases, as noted in the preceding chapter (See Figs. 6 and 7).

3.3.5. Study of Spectra

The amplitude spectra of wing bending moment, acceleration for A2 and pressure for K1 and K3 within the band 0-300 Hz are given for 2° and 8° in Figs. 18, 19 and 20[1].

(The notation $\sqrt{\overline{\Delta Q^2}_{\Delta f}}$ given for the ordinate indicates that the effective value for quantity Q has been assumed to be within the frequency band f - f + Δf.) An examination of these figures leads

[1]The spectra presented relate to the second assembly (see Fig. 22).

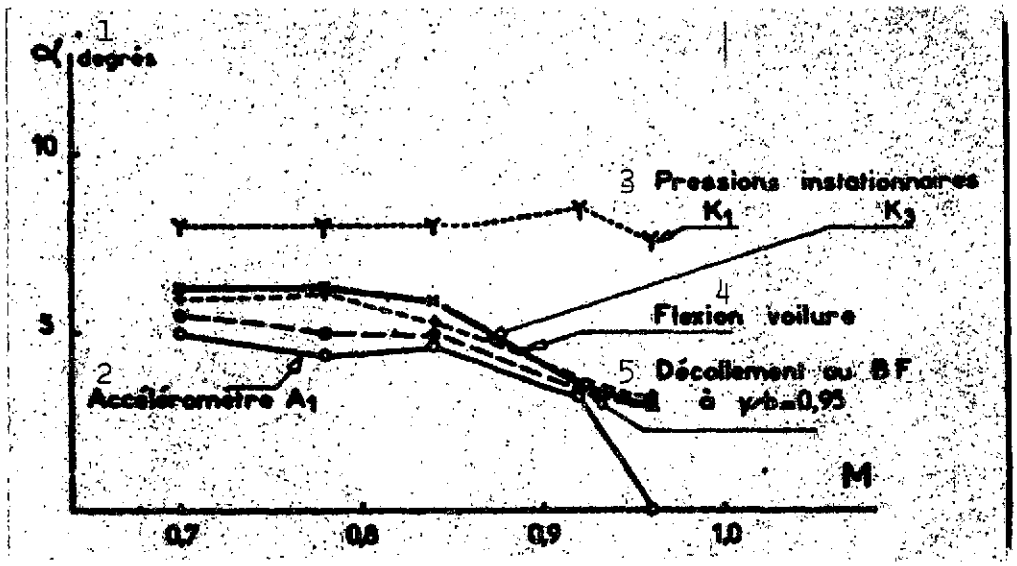

Fig. 17. Angles of attack for divergence obtained with various detection methods. $R_{\bar{c}} = 2.5 \cdot 10^6$.

Key: 1. Degrees.
2. A1 accelerometer.
3. Nonstationary pressure.
4. Wing bending.
5. Separation at trailing edge at y/b = 0.95.

to the following observations:

-- There is a considerable difference in level between 2°, where there is no separation, and 8°, where separation and buffeting are well established.

-- The energy of the aerodynamic excitation is distributed throughout the entire frequency range, while the energy of the response of the structure is concentrated around a few frequencies corresponding to the characteristic vibration modes of the wing, principally around 17 Hz, the frequency of the first wing bending mode.

-- In addition, the wing bending response occurs almost exclusively in this mode.

Within the band 0-500 Hz, Fig. 21 furnishes a more complete idea of the nature of variations in the pressure spectrum as the angle of attack increases, at Mach 0.84. The spectra at low angles of attack (0.2° and 4°) are characterized by low-level white noise, on which are superimposed more or less widely spaced lines whose intensity decreases as the angle of attack increases.

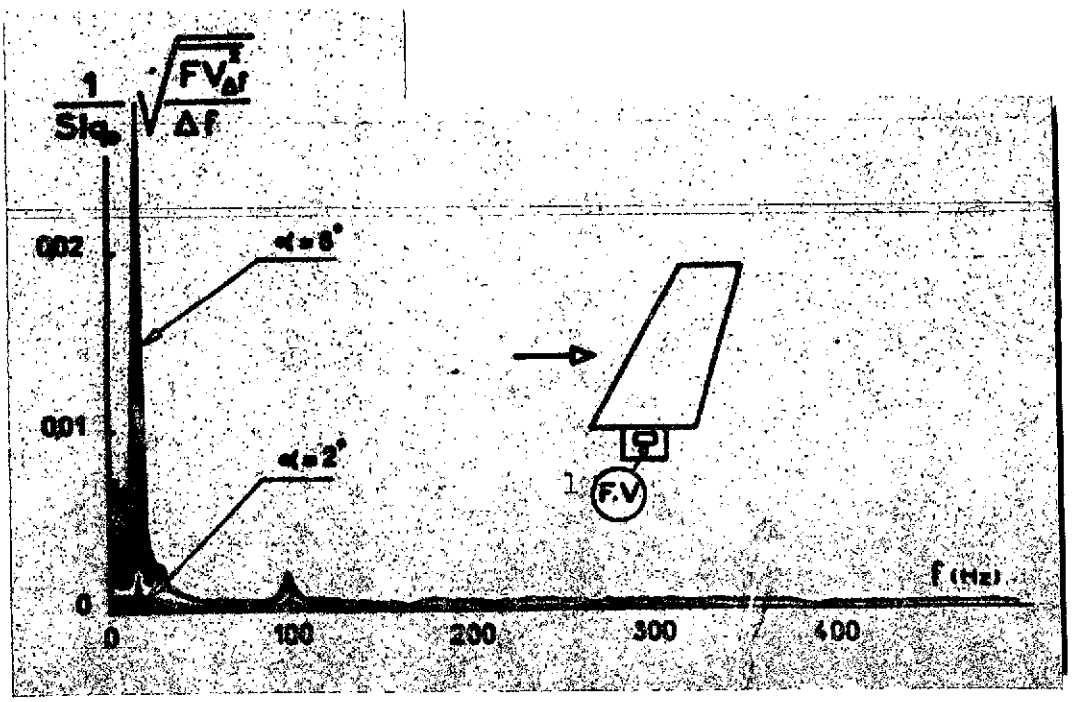

Fig. 18. Spectra of wing bending moment. M = 0.84. $R_{\bar{c}} \cong 2.5 \cdot 10^6$.

Keye 1. Wing bending.

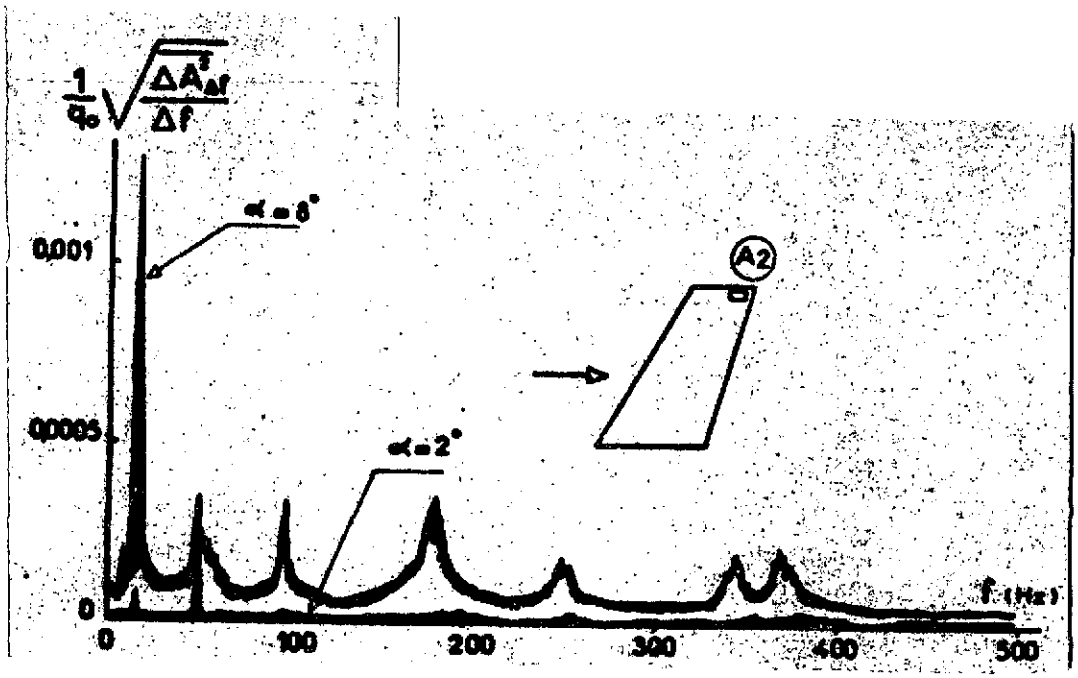

Fig. 19. Spectra of acceleration fromAA2. M = 0.84. $R_c = 2.5 \cdot 10^6$.

The same phenomenon is observed at a higher intensity at lower Mach numbers, but it disappears at higher Mach numbers. These lines correspond to the lines observed in examining wind tunnel noise spectra [3]. /12

Given the rate of pressure distribution at an angle of attack of 0° (Fig. 3), it may be assumed that at low Mach numbers the transition occurs well to the rear of the airfoil, in a low gradient region. The pressure on the wing at a low angle of attack is probably influenced by wind tunnel noise through the effects of the transition.

At an angle of attack of 6° buffeting begins to occur and the spectrum bulges throughout the entire frequency range.

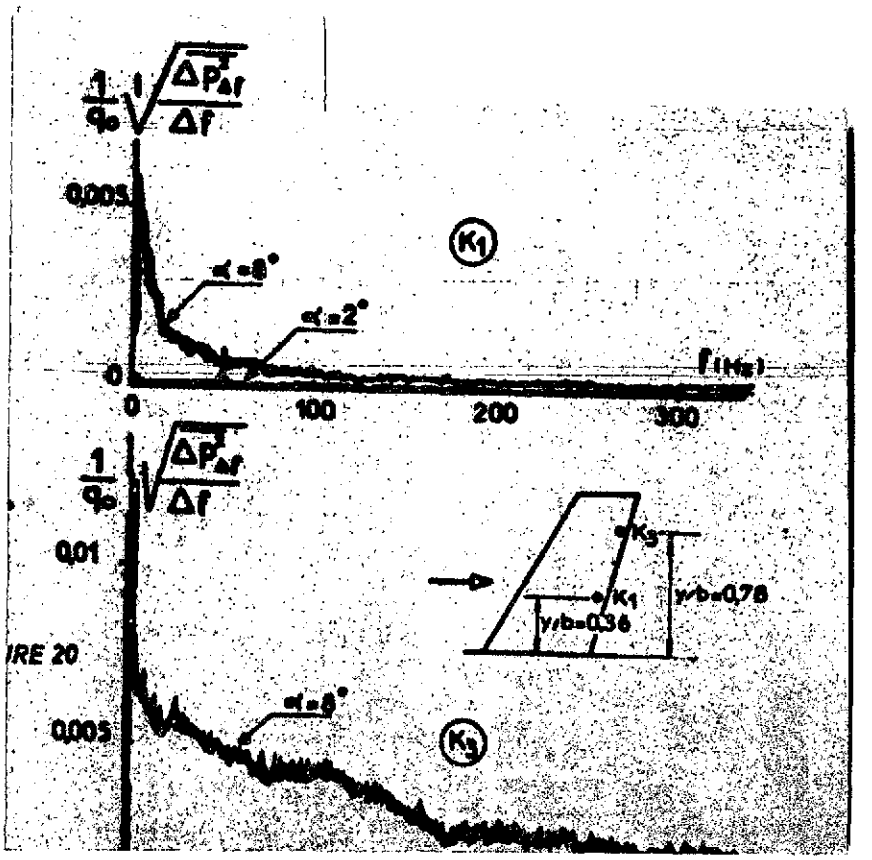

Fig. 20. Spectra of nonstationary pressure. M = 0.84. $R_{\bar{c}} = 2.5 \cdot 10^6$.

Between angles of attack of 6° and 8°, buffeting develops solely within the frequency range 0-1500 Hz.

Beyond 8 , the separation becomes organized and the buffeting level decreases uniformly over the entire spectrum.

3.4. Influence of Assembly Type

To attempt to determine what influence the movement of the model might have on the aerodynamics, a second series of tests was performed with a modifed wing assembly (Fig. 22).

In the second assembly, the wing was secured on a balance

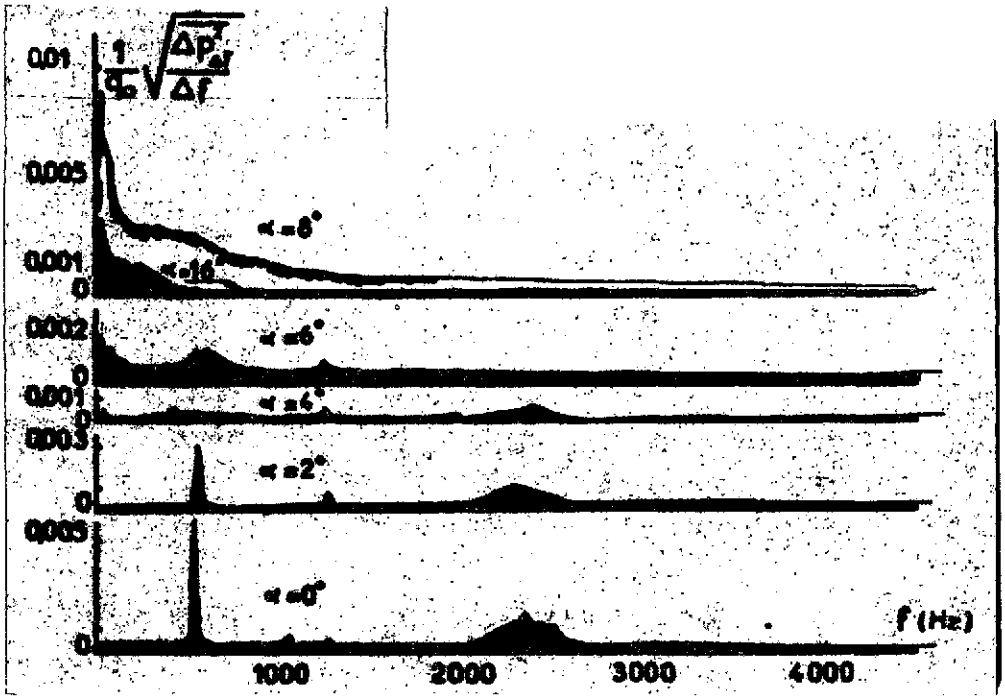

Fig. 21. Spectra of pressure amplitude for K4. M = 0.84. $R_{\bar{c}} = 2.5 \cdot 10^6$.

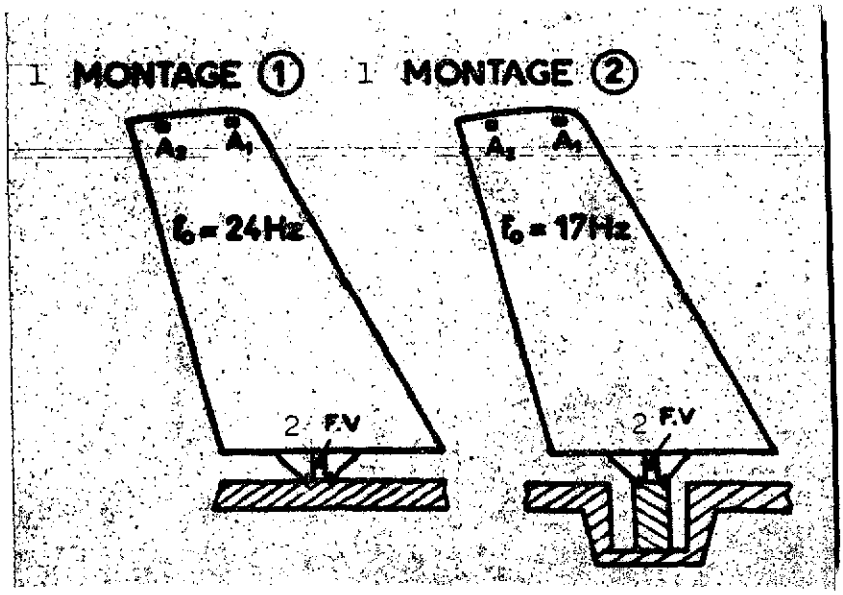

Fig. 22. Configuration of the two assembly types.
Key: 1. Assembly. 2. Wing bending.

which had the effect of decreasing the frequency of the first bending mode for the assembly from 24 to 17 Hz. The response of the structure to a buffeting regime was found to undergo fairly heavy changes both in frequency (Fig. 23) and level (Fig. 24). On the other hand, the aerodynamic magnitudes remained remarkably constant:

-- The trailing edge pressure divergence curves were identical (Fig. 25).

-- The spectra of nonstationary pressure within the range 0-500 Hz were the same.

-- Finally, the effective nonstationary pressure values were extremely close (Fig. 26).

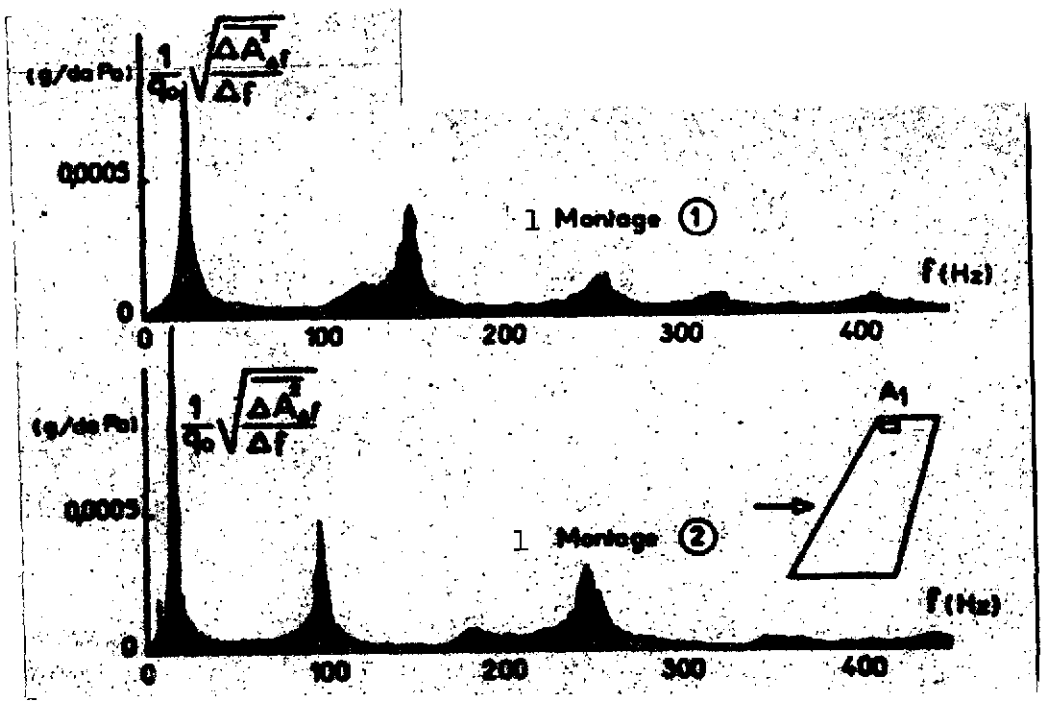

Fig. 23. Spectra of acceleration from A1. M = 0.84. $R_c = 2.5 \cdot 10^6$. $\alpha = 8°$.

Key: 1. Assembly.

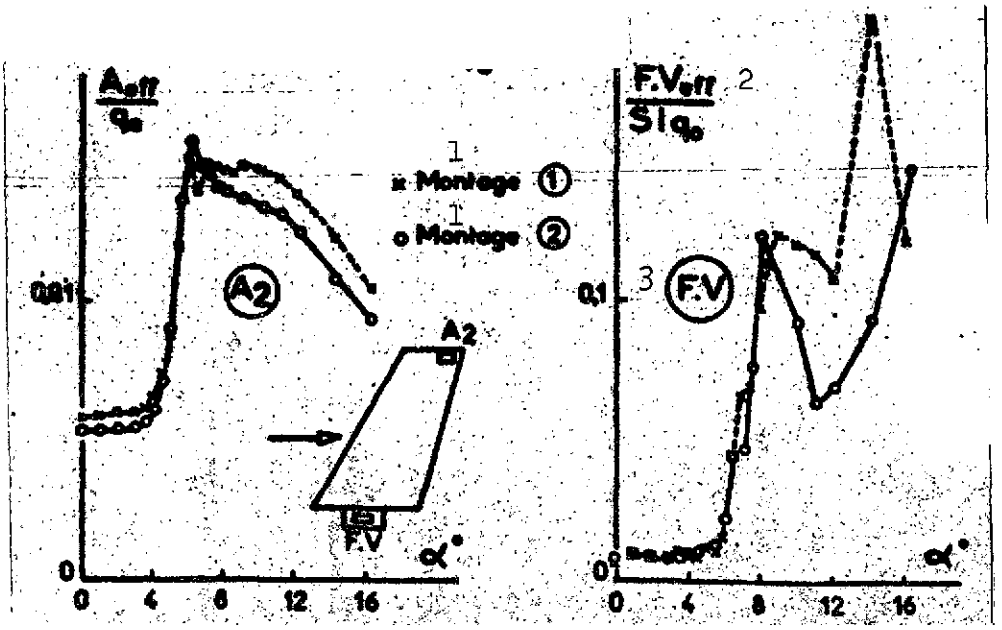

Fig. 24. Comparison of nonstationary mechanical responses of the two assemblies used. M = 0.84. $R_{\bar{c}} = 2.5 \cdot 10^6$.

Key: 1. Assembly. 2. Effective wing bending. 3. Wing bending.

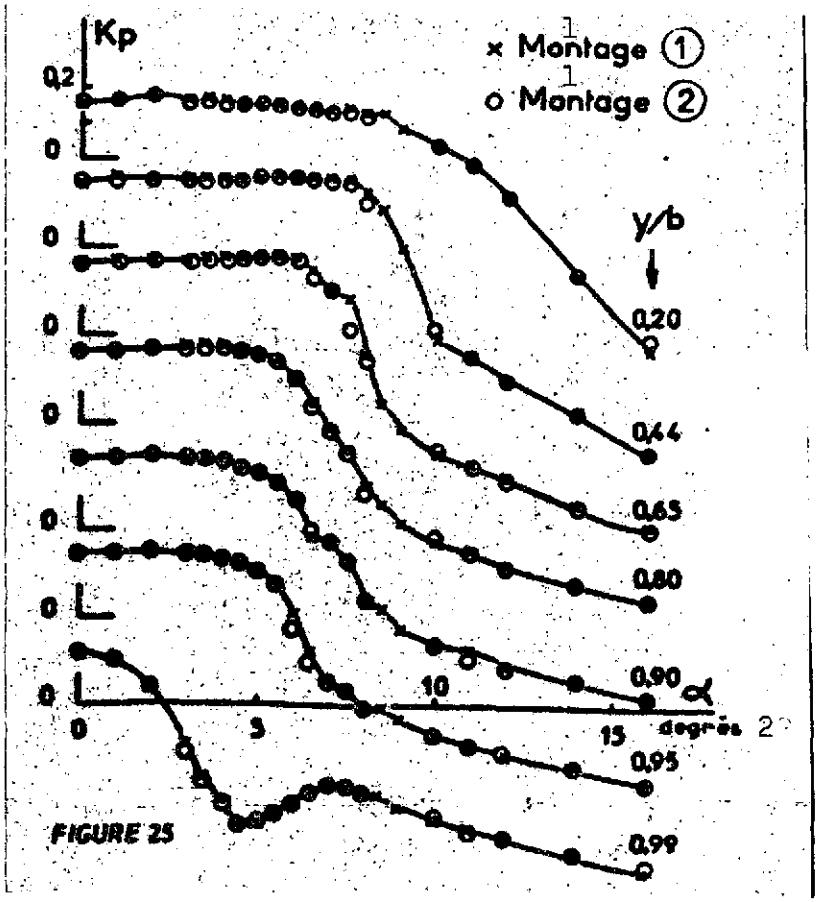

Fig. 25. K_p for trailing edge. M = 0.84. $R_{\bar{c}} = 2.5 \cdot 10^6$.

Key: 1. Assembly.
22. Degrees.

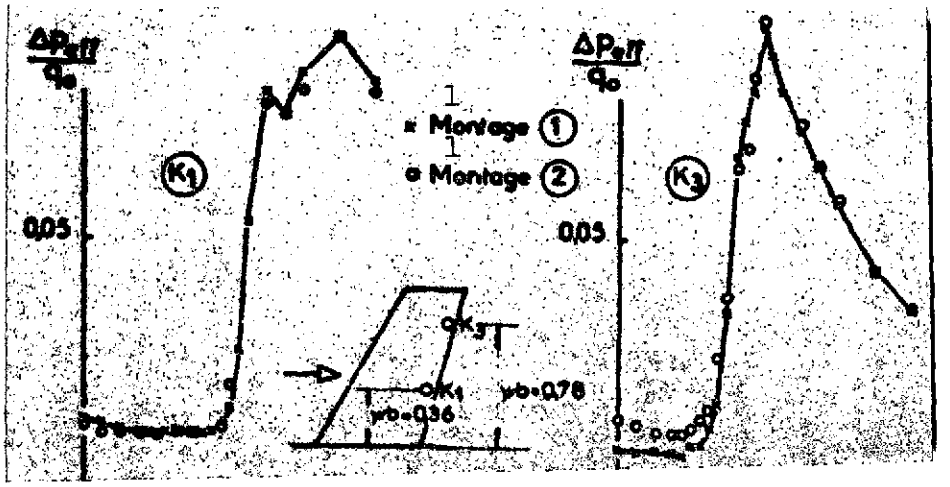

Fig. 26. Comparison of measured nonstationary pressures for the two assemblies used. M = 0.84. $R_{\bar{c}} = 2.5 \cdot 10^6$.

Key: 1. Assembly.

4. Conclusions

The study which has just been presented is far from complete; there is still much work to be done in exploiting and analyzing data, and anyisonclusions at this stage would be somewhat premature.

Nevertheless, in view of the data obtained so far it may be stated that the movement of the model apparently has no appreciable influence on the aerodynamics. However, this point must still be checked by testing models with wider structural variations.

If this theory is confirmed, it should be possible to develop a method for quantizing buffeting based on the measurement of nonstationary pressure on the wing.

REFERENCES

1. Dyment, A., and Vincent de Paul, M., "Recherches sur les profils d'ailes en écoulement subsonique élevé," Aeronautique et Astronautique No. 19 (1970).

2. Ledoux, M., and Monnerie, B., "Etude théorique et expérimentale d'une aile en flêche à faible vitesse et dans un large domaine d'incidences," paper presented at the 9th Colloquium on Applied Aerodynamics of the AAAF (1972).

3. Canu, M., "Qualification de la turbulence et du bruit interne en subsonique et en transsonique dans les souffleries S2 et S2 de Modane," paper presented at the 10th Colloquium on Applied Aerodynamics of the AAAF (1973).